Mechanism of Water Oxidation by the μ-Oxo Dimer $[(bpy)_2(H_2O)Ru^{III}ORu^{III}(OH_2)(bpy)_2]^{4+}$

Robert A. Binstead, Chris W. Chronister, Jinfeng Ni, Chris M. Hartshorn, and Thomas J. Meyer*

Contribution No. 3290 from the Department of Chemistry, Venable Hall, The University of North Carolina, Chapel Hill, North Carolina 27599-3290

Received September 8, 1999. Revised Manuscript Received June 7, 2000

Abstract: The kinetics and mechanism of Ce^{IV} oxidation of the water oxidation catalyst $[(bpy)_2(H_2O)Ru^{III}ORu^{III}(OH_2)(bpy)_2]^{4+}$ (**1**, $Ru^{III}ORu^{III}$) have been investigated by UV−visible measurements with application of global analysis. The reaction proceeds by stepwise oxidation of $Ru^{III}ORu^{III}$ to $Ru^{V}ORu^{V}$ with oxidation of $Ru^{IV}ORu^{III}$ the slow step. $Ru^{V}ORu^{V}$ has been identified as an intermediate by the appearance of its ClO_4^- salt as a black suspension in concentrated solutions at 5 °C. It is the key intermediate in water oxidation. The mechanism may involve a bimolecular step and formation of a peroxo-bridged intermediate. Catalytic water oxidation is greatly retarded after just a few catalytic cycles because of anation induced by O_2 evolution.

Introduction

The oxidation of water to dioxygen is the terminal step in photosystem II in the natural photosynthetic apparatus.[1] It is a thermodynamically demanding reaction with $E° = 1.23$ V for the O_2/H_2O couple and 0.81 V at pH 7. It is also mechanistically demanding since it requires the loss of four electrons and four protons with the concomitant formation of an O−O bond.

$$2H_2O \rightarrow O_2 + 4H^+ + 4e^- \quad (1)$$

Considerable progress has been made in elucidating structure and possible water oxidation mechanisms at the four-manganese cluster site of the Oxygen Evolving Complex (OEC) of photosystem II.[2−4] The mechanistic importance of proton loss and proton-coupled electron transfer have also been discussed.[5,6] EXAFS studies have revealed that the Mn tetramer consists of two linked di-μ-oxo dimeric units.[2,7] In a recent theoretical paper it was proposed that the key O−O bond formation step involves water attack on the oxyl oxygen of a reactive manganese oxo site.[4]

There are few well-defined molecules which act as catalysts toward water oxidation. This is not surprising given the thermodynamic and mechanistic requirements and the demand that the catalytic site be imbedded in an oxidatively stable coordination environment. Nonphotosynthetic water oxidation has been reviewed by Rüttinger and Dismukes.[8] Since that paper catalytic water oxidation by a μ-oxo manganese dimer with HOCl as the terminal oxidant has been reported.[9]

Among the very few water oxidation catalysts is the μ-oxo Ru^{III} dimer $[(bpy)_2(H_2O)Ru^{III}ORu^{III}(OH_2)(bpy)_2]^{4+}$ (**1**) and its derivatives.[10−22] Based on the results of pH-dependent electrochemical measurements, the basic structural unit is retained in oxidation states from $Ru^{III}ORu^{III}$ to $Ru^{V}ORu^{V}$.[11] Water oxidation is triggered by oxidation to $Ru^{V}ORu^{V}$. Oxygen evolution is initially rapid but slows considerably after passage through even a few catalytic cycles. Oxidation states $Ru^{III}ORu^{III}$ and $Ru^{IV}ORu^{III}$ have been characterized by X-ray crystallography,[11,23] and resonance Raman and EPR spectra have been reported for these and the higher oxidation state $Ru^{V}ORu^{IV}$ and $Ru^{V}ORu^{V}$ forms.[15,16,23]

A question of importance is the mechanism by which the μ-oxo dimer oxidizes water to dioxygen. It is highly complex since it involves stepwise, four-electron oxidation from $Ru^{III}ORu^{III}$ to $Ru^{V}ORu^{V}$ followed by water oxidation. There are additional complications from anation induced by O_2 evolution and cross-electron transfer between nonadjacent oxidation states. The unraveling of this mechanism is a major tour de force in demonstrating the power of global analysis techniques in unraveling complex kinetic schemes.

(1) Debus R. J. *Biochim. Biophys. Acta* **1992**, *1102*, 269.
(2) Yachandra, V. K.; Sauer, K.; Klein, M. P. *Chem. Rev.* **1996**, *96*, 2927.
(3) Lindberg, K.; Andréasson, L.-E. *Biochemistry* **1996**, *35*, 14259.
(4) Siegbahn, P. E. M.; Crabtree, R. H. *J. Am. Chem. Soc.* **1999**, *121*, 117.
(5) Tommos, C.; Babcock, G. T. *Acc. Chem. Res.* **1998**, *31*, 18.
(6) Hoganson, C. W.; Babcock, G. T. *Science* **1997**, *277*, 1953.
(7) Kirby, J. A.; Robertson, A. S.; Smith, J. P.; Cooper, S. R.; Klein, M. P. *J. Am. Chem. Soc.* **1981**, *103*, 5529.
(8) Rüttinger, W.; Dismukes, G. C. *Chem. Rev.* **1997**, *97*, 1.
(9) Limburg, J.; Vrettos, J. S.; Liable-Sands, L. M.; Rheingold, A. L.; Crabtree, R. H.; Brudvig, G. W. *Science* **1999**, *283*, 1524.
(10) Gersten, S. W.; Samuels, G. J.; Meyer, T. J. *J. Am. Chem. Soc.* **1982**, *104*, 4029.
(11) Gilbert, J. A.; Eggleston, D. S.; Murphy, W. R., Jr.; Geselowitz, D. A.; Gersten, S. W.; Hodgson, D. J.; Meyer, T. J. *J. Am. Chem. Soc.* **1985**, *107*, 3855.
(12) Raven, S. J.; Meyer, T. J. *Inorg. Chem.* **1988**, *27*, 4478.
(13) Geselowitz, D. A.; Meyer, T. J. *Inorg. Chem.* **1990**, *29*, 3894.
(14) Hurst, J. K.; Zhou, J.; Lei, Y. *Inorg. Chem.* **1992**, *31*, 1010.
(15) Lei, Y.; Hurst, J. K. *Inorg. Chem.* **1994**, *33*, 4460.
(16) Lei, Y.; Hurst, J. K. *Inorg. Chim. Acta* **1994**, *226*, 179.
(17) Chronister, C. W.; Binstead, R. A.; Ni, J.; Meyer, T. J. *Inorg. Chem.* **1997**, *36*, 3814.
(18) Rotzinger, F. P.; Munavalli, S.; Comte, P.; Hurst, J. K.; Gratzel, M.; Pern, F. J.; Frank, A. J. *J. Am. Chem. Soc.* **1987**, *109*, 6619.
(19) Nazeeruddin, M. K.; Rotzinger, F. P.; Comte, P.; Gratzel, M.; Pern, F. J.; Frank, A. J. *J. Chem. Soc., Chem. Commun.* **1988**, 872.
(20) Comte, P.; Nazeeruddin, M. K.; Rotzinger, F. P.; Frank, A. J.; Gratzel, M. *J. Mol. Catal.* **1989**, *52*, 63.
(21) Petach, H. H.; Elliott, C. M. *J. Electrochem. Soc.* **1992**, *139*, 2217.
(22) Lai, Y.-K.; Wong, K.-Y. *J. Electrochem. Soc.* **1995**, *380*, 193.
(23) Schoonover, J. R.; Ni, J.; Roecker, L.; White, P. S.; Meyer, T. J. *Inorg. Chem.* **1996**, *35*, 5885.

10.1021/ja993235n CCC: $19.00
Published on Web 08/16/2000

We present here an account of the mechanism of catalytic water oxidation by **1**. It is constructed from kinetic results reported, in part, in an earlier communication and from an even earlier ^{18}O-labeling study.[13,17] It has important implications for the design of water oxidation catalysts and, more generally, for our understanding of oxidative chemical reactivity.

Experimental Section

Materials. Water was purified in a Barnstead Nanopure purification system. Due to the high reactivity of the higher oxidation states of the μ-oxo bridged dimer, all glassware was washed with 0.5 M $H_2Ce(ClO_4)_6$ in 6 M perchloric acid (GFS) prior to use and rinsed with copious amounts of purified water. Stock solutions of Ce^{IV} for kinetic and stoichiometry measurements were prepared from $(NH_4)_2Ce(ClO_4)_6$ (99.3%, Aldrich). Perchloric acid (75%) was purchased from GFS and trifluoromethanesulfonic acid (CF_3SO_3H, >99.99%) was purchased from Aldrich. Solutions of sodium trifluoromethanesulfonate were prepared by neutralization of CF_3SO_3H with NaOH (99.99%, Aldrich). All other reagents were used without further purification.

The quality and purity of trifluoromethanesulfonic acid used in the stoichiometry experiments greatly influenced the results. When reaction of **1** (5×10^{-5} M) with 30 equiv of Ce^{IV} in 1 M CF_3SO_3H prepared from 98% CF_3SO_3H from Aldrich was monitored spectrophotometrically, the UV−visible spectrum remained nearly unchanged for ~600 s after which the dimer entered the catalytic water oxidation cycle (see below). After consumption of Ce^{IV}, a second 30 equiv of Ce^{IV} was added and the catalytic cycle was entered immediately without inhibition. We attribute this behavior to reducing impurities in the trifluoromethanesulfonic acid with inhibition occurring as the higher oxidation state forms, $Ru^{V}ORu^{IV}$ and $Ru^{V}ORu^{V}$ (see below), oxidize the impurity or impurities more rapidly than water. The extent of this behavior was found to depend on the acid sample with one lot (Aldrich, >99.99%) sufficiently impurity free to be used without further purification. A second lot contained an impurity that was removed by vacuum distillation from a mixture of **1** and an excess of Ce^{IV}.

Preparations. *cis,cis*-$[(bpy)_2(H_2O)Ru^{III}ORu^{III}(H_2O)(bpy)_2](ClO_4)_4$, **1**$(ClO_4)_4$, and *cis,cis*-$[(bpy)_2(HO)Ru^{IV}ORu^{III}(H_2O)(bpy)_2](ClO_4)_4$, **2**$(ClO_4)_4$, were prepared as described previously.[11] ***Warning***: *Perchlorate salts are hazardous because of the possibility of explosion.*

$[(bpy)_2(O)Ru^{V}ORu^{IV}(O)(bpy)_2]^{3+}$ ($Ru^{V}ORu^{IV}$) in Situ. Solutions containing $Ru^{V}ORu^{IV}$ were prepared by electrolysis of $[(bpy)_2(HO)Ru^{IV}ORu^{III}(OH)(bpy)_2]^{3+}$ (1×10^{-4} M) in 0.1 M $NaCF_3SO_3$ in an ice bath at an applied potential of 730 mV vs Hg/Hg_2SO_4 (~1.1 V vs SSCE). The electrolysis was monitored by UV/vis spectrophotometry to ascertain when oxidation to $Ru^{V}ORu^{IV}$ ($\lambda_{max} = 496$ nm, $\epsilon = 8000$ M^{-1} cm^{-1}) was complete. For experiments at pH 5−6, the electrolysis solution contained a mixture of $NaCF_3SO_3$ and $NaCH_3CO_2$. This buffer was chosen because of the availability of high-purity $NaCH_3CO_2$.

Instrumentation. UV/vis spectra were recorded on a Hewlett-Packard Model 8452A diode-array spectrophotometer. Stopped-flow experiments were performed on a Hi-Tech SF-51 stopped-flow apparatus equipped with a diode array detector by using an On Line Instrument System (OLIS) stopped-flow program for data acquisition and analysis. Photoreduction of the higher oxidation states was avoided by use of a total of 2.0 OD units of neutral density attenuation for the Xenon light source. Data were processed by use of the program SPECFIT (Spectrum Software Associates, Chapel Hill, NC). Resonance Raman spectra were obtained in frozen solutions with a Princeton Instruments IG-CCD detector coupled to a Spex triplemate operated in spectrograph mode. A Copenhagen Radiometer PHM62 Standard pH meter was used to measure solution pH.

Electrochemical measurements were performed on EG&G Princeton Applied Research model 264A and 273 potentiostats. Voltammetric measurements were made with a glassy carbon electrode (BAS), a platinum wire counter electrode, and a Hg/Hg_2SO_4 reference electrode (0.41V vs SSCE). Electrolyses and coulometry were conducted in a three-compartment cell by using a reticulated vitreous carbon working electrode, a platinum flag counter electrode, and a Hg/Hg_2SO_4 reference electrode.

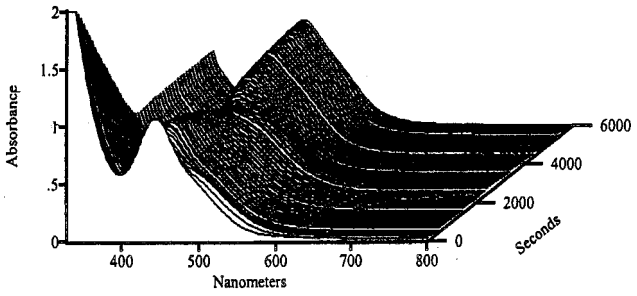

Figure 1.

For oxygen-evolution experiments the amount of oxygen produced was monitored by using an Orion Research model 97-08 O_2 electrode. The measurements were made on solutions that had been purged with argon for 30 min. The reactions were initiated by adding solutions containing Ce^{IV} through a septum. Measurements were taken of the oxygen produced in the headspace in the closed cell. The amount of oxygen produced was calculated based on the known headspace volume. The amount of oxygen evolved was also determined by gas chromatography. The headspace was monitored at the conclusion of the experiments and compared with a calibration curve to determine the amount of oxygen produced. These samples were run on a Hewlett-Packard 5142 Gas Chromatograph equipped with a 5 Å molecular sieve column and a FID.

Results

In earlier work the oxidation−reduction chemistry of *cis,cis*-$[(bpy)_2(H_2O)Ru^{III}ORu^{III}(H_2O)(bpy)_2]^{4+}$ (**1**) was investigated as a function of pH by cyclic voltammetry.[11] Direct evidence was obtained in these experiments for oxidation to *cis,cis*-$[(bpy)_2(HO)Ru^{IV}ORu^{III}(H_2O)(bpy)_2]^{4+}$ (**2**) and the higher oxidation states $[(bpy)_2(O)Ru^{V}ORu^{IV}(O)(bpy)_2]^{3+}$ and $[(bpy)_2(O)Ru^{V}ORu^{V}(O)(bpy)_2]^{4+}$. The proton content was inferred from the pH-dependent electrochemical data. These complexes have an extensive pH-dependent electrochemistry because of the gain and loss of protons from the coordinated water molecules and an increase in acidity upon oxidation. Based on the results of electrochemical and spectrophotometric pH titrations, $pK_{a1} = 5.9$ and $pK_{a2} = 8.3$ for $Ru^{III}ORu^{III}$ and $pK_{a1} = 0.4$ and $pK_{a2} = 3.2-3.3$ for $Ru^{IV}ORu^{III}$.

For convenience, the various oxidation states will be referred to as $Ru^{III}ORu^{III}$, $Ru^{IV}ORu^{III}$, $Ru^{V}ORu^{IV}$, and $Ru^{V}ORu^{V}$ and the "missing" oxidation state as $Ru^{IV}ORu^{IV}$ (see below) without reference to proton content. Because of strong electronic coupling across the μ-oxo bridge, the mixed-valence forms may be delocalized.

Catalysis of Water Oxidation. The catalytic oxidation of water was investigated by addition of 17−100 equiv of Ce^{IV} to solutions containing $Ru^{IV}ORu^{III}$ (3×10^{-5} to 8×10^{-4} M) in 1 M $HClO_4$ or CF_3SO_3H. The loss of Ce^{IV} was monitored by diode array UV/vis spectrophotometry and the appearance of O_2 by use of an O_2 electrode. The results of a typical experiment are illustrated in the spectral-time trace in Figure 1. In Figure 2 are shown absorbance−time changes at the λ_{max} for Ce^{IV} at 360 nm and the evolution of O_2 with time.

The evolution of O_2 was measured in a series of experiments at varying Ce^{IV} to $Ru^{III}ORu^{III}$ or $Ru^{IV}ORu^{III}$ ratios and shown to be stoichiometric or nearly stoichiometric based on Ce^{IV} added. In a typical experiment with $[Ru^{III}ORu^{III}] = 2.0 \times 10^{-4}$ M and $[Ce^{IV}] = 6.0 \times 10^{-3}$ M after mixing, the amount of O_2 produced was 96% of that predicted based on the amount of Ce^{IV} added. Under these conditions, the turnover number per hour, measured as the number of moles of O_2 produced per mole of dimer, was 11.

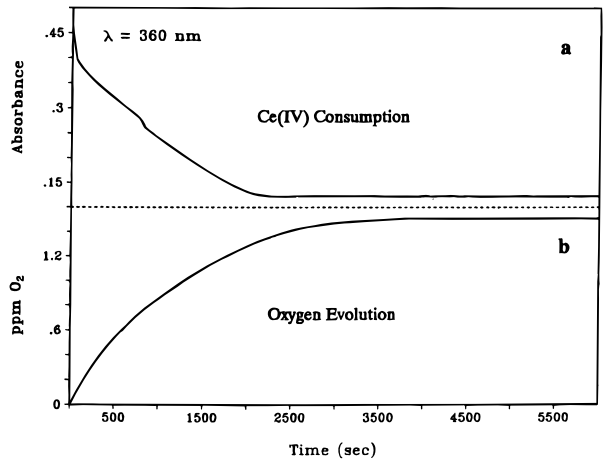

Figure 2.

As measured in this way, the apparent turnover number is deceiving. As discussed below, the oxidation of water occurs within the initial, absorbance−time change in Figure 2, and is complete within seconds. After the consumption of ∼4 equiv of Ce^{IV}, the disappearance of Ce^{IV} begins to slow, with pseudo-zero-order kinetics observed after 6−8 equiv. These observations show that much of the catalyst is deactivated after only 1−2 cycles of water oxidation. The effect is reversible. After solutions were aged for several hours, the initial, fast reaction is reproduced but, once again, lapses into zero-order kinetics upon addition of excess Ce^{IV}.

The pseudo-zero-order slopes at pH 0 for the slow, second stage in Figure 2b yielded rate constants of 0.01 (CF_3SO_3H) and 0.025 M s^{-1} ($HClO_4$). As reported by Lei and Hurst, but with $Co(H_2O)_6^{3+}$ as the oxidant,[16] these rate constants are linearly dependent on $[Ru^{III}ORu^{III}]$.

Under similar conditions at pH 1 (μ = 0.1, CF_3SO_3H, 25 °C), Ce^{IV} is consumed more rapidly. While the kinetics are still pseudo-zero order, the curvature in the kinetic traces is marked (Figure 1S in Supporting Information) consistent with a contribution to the rate-limiting behavior by Ce^{IV} oxidation. Addition of 0.9 M $NaCF_3SO_3$ caused precipitation of the catalyst so that direct comparison at constant ionic strength was not possible.

Oxidation of $Ru^{III}ORu^{III}$ to $Ru^{V}ORu^{V}$. Kinetic studies on the stepwise oxidation of $Ru^{III}ORu^{III}$ to $Ru^{V}ORu^{V}$ were conducted with stoichiometric or less than stoichiometric amounts of added Ce^{IV} with UV−visible monitoring to avoid complications arising from entry into the water oxidation cycle.

In the previous communication, a mechanism was proposed that was derived by application of global analysis and singular value decomposition (SVD) to multiple wavelength, absorbance−time data. As shown in Scheme 1, it proposed stepwise oxidation of $Ru^{III}ORu^{III}$ to $Ru^{V}ORu^{V}$.[17] The kinetic analysis provided rate constants or estimates of rate constants for each step. Scheme 1 is a slightly modified version of the earlier scheme. It and the associated rate constants are given here as a summary and guide to understanding the mechanism of water oxidation.

All of the rate constants in the scheme refer to second-order processes unless otherwise noted. The values are cited at 25 °C in 1 M $HClO_4$. For the sake of clarity these reactions are not balanced in charge or proton content. For example, the balanced reaction for eq a in Scheme 1 is,

$$cis,cis\text{-}[(bpy)_2(H_2O)Ru^{III}ORu^{III}(H_2O)(bpy)_2]^{4+} + Ce^{IV} \rightarrow cis,cis\text{-}[(bpy)_2(OH)Ru^{IV}ORu^{III}(H_2O)(bpy)_2]^{4+} + H^+ + Ce^{III}$$

Scheme 1

(a) $Ru^{III}ORu^{III} + Ce^{IV} \xrightarrow{k_1\ (2\times10^4)} Ru^{IV}ORu^{III} + Ce^{III}$

(b) $Ru^{IV}ORu^{III} + Ce^{IV} \xrightarrow{k_2\ (15)} Ru^{IV}ORu^{IV} + Ce^{III}$

(c) $Ru^{IV}ORu^{III} + Ru^{V}ORu^{IV} \underset{k_{-3}\ (\geq10^5)}{\overset{k_3\ (7.3\times10^3)}{\rightleftharpoons}} 2\,Ru^{IV}ORu^{IV}$

(d) $Ru^{IV}ORu^{IV} + Ce^{IV} \xrightarrow{k_4\ (\geq10^5)} Ru^{V}ORu^{IV} + Ce^{III}$

(e) $Ru^{V}ORu^{IV} + Ce^{IV} \xrightarrow{k_5\ (\geq10^2)} Ru^{V}ORu^{V} + Ce^{III}$

(f) $Ru^{V}ORu^{V} + 2\,H_2O$ (first order) $\xrightarrow{k_6\ (\geq1\ s^{-1})} Ru^{III}ORu^{III} + O_2$

(f′) $2\,Ru^{V}ORu^{V} + 2\,H_2O$ (second order) $\xrightarrow{k_6'\ (>2\times10^4)} Ru^{IV}ORu^{III} + Ru^{V}ORu^{IV} + O_2$

(g) $Ru^{III}ORu^{III} + Ru^{V}ORu^{IV} \xrightarrow{k_7\ (\geq10^6)} Ru^{IV}ORu^{III} + Ru^{IV}ORu^{IV}$

(h) $2\,Ru^{V}ORu^{IV} \underset{k_{-8}\ (<22)}{\overset{k_8\ (22)}{\rightleftharpoons}} Ru^{IV}ORu^{IV} + Ru^{V}ORu^{V}$

Table 1. Rate Constants for Ce^{IV} Oxidation of $Ru^{III}ORu^{III}$ at 25 °C

medium	k_1 ($M^{-1}\ s^{-1}$)[a]	k_{H_2O}/k_{D_2O}
1.0 M $HClO_4$	1.6×10^3	
1.0 M CF_3SO_3H	1.8×10^3	0.87
0.1 M $HClO_4$	5.9×10^2	
0.1 M CF_3SO_3H	7.2×10^2	0.82

[a] ±20%.

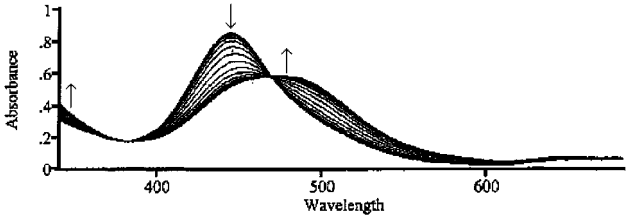

Figure 3.

$Ce^{IV} + Ru^{III}ORu^{III} \rightarrow Ce^{III} + Ru^{IV}ORu^{III}$. The kinetics of Ce^{IV} oxidation of $Ru^{III}ORu^{III}$ to $Ru^{IV}ORu^{III}$ were investigated at various concentrations of dimer but always with $[Ce^{IV}] < [Ru^{III}ORu^{III}]$ to avoid complications from oxidation past $Ru^{IV}ORu^{III}$. The rate law is first order in Ce^{IV} and first order in $Ru^{III}ORu^{III}$. The results are summarized in Table 1. Notable features that appear in the data include the decrease in k_1 by ∼2 from $[H^+]$ = 1 to 0.1 M and the inverse kinetic isotope effect of 0.8−0.9 in $DClO_4$ compared to that in $HClO_4$.

The value of k_1 derived by direct measurement is less than the value in Scheme 1 derived by global analysis. The difference is presumably a reflection of the complexity of the multistep scheme treated by global analysis with its kinetically overlapping reactions.

$2Ce^{IV} + Ru^{IV}ORu^{III} \rightarrow 2\ Ce^{III} + Ru^{V}ORu^{IV}$. In a typical experiment, the addition of 1 equiv of Ce^{IV} to $Ru^{IV}ORu^{III}$ (3.5×10^{-5} M, λ_{max} = 446 nm) at pH 0 in $HClO_4$ at 25 °C resulted in partial oxidation to $Ru^{V}ORu^{IV}$ (λ_{max} = 484 nm), with no clear evidence for an intermediate. Addition of 2 equiv of Ce^{IV} resulted in nearly quantitative oxidation to $Ru^{V}ORu^{IV}$. Spectral changes with time at various intervals from the time of mixing to 200 s are shown in Figure 3. Analysis of these data by singular value decomposition revealed two principal colored species with evidence for a third. The concentration profiles with time are shown in Figure 4 and the time and spectral eigenvectors from singular value decomposition in Supplemen-

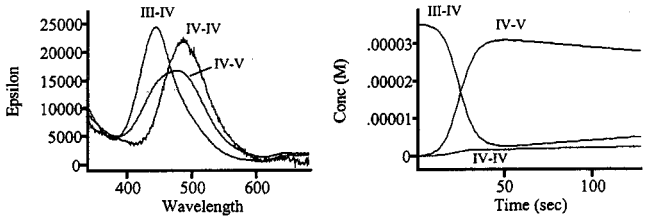

Figure 4.

tary Figures 2S and 3S. With 3−10 equiv of added Ce^{IV}, further oxidation occurred as the system entered the catalytic cycle for water oxidation.

The shape of the initial autocatalytic portion of the concentration−time profiles in Figure 4 provides two of the rate constants in the final kinetic model in Scheme 1 (k_2, k_3), while the tailing portion that appears after the consumption of Ce^{IV} yields k_8 for the disproportionation of $Ru^{V}ORu^{IV}$ which is slow. The value obtained for k_8 is in satisfactory agreement with results obtained using solutions in which $Ru^{V}ORu^{IV}$ was generated independently, see below. The value of k_{-8} is unknown, and unimportant in the model.

An interesting feature of the full kinetic model is that it predicts the buildup of a one-electron intermediate, $Ru^{IV}ORu^{IV}$, but in small amount ($(1-2) \times 10^{-6}$ M in maximum amount under the conditions in Figure 4). This intermediate could be $Ru^{V}ORu^{III}$ rather than $Ru^{IV}ORu^{IV}$ (see Discussion), but for convenience will be referred to as $Ru^{IV}ORu^{IV}$. In electrochemical measurements only the two-electron, $Ru^{V}ORu^{IV}/Ru^{IV}ORu^{III}$ couple is observed showing that $Ru^{IV}ORu^{IV}$ is unstable toward disproportionation into $Ru^{V}ORu^{IV}$ and $Ru^{IV}ORu^{III}$.[11] The kinetic model also predicts that neither the highest oxidation state, $Ru^{V}ORu^{V}$ ($<10^{-7}$ M), nor the lowest oxidation state, $Ru^{III}ORu^{III}$ ($<10^{-8}$ M), exist in significant amounts during the water oxidation cycle.

The fact that the predicted spectrum of $Ru^{IV}ORu^{IV}$ in Figure 4 appears to be a linear combination of the $Ru^{IV}ORu^{III}$ and $Ru^{V}ORu^{IV}$ spectra in the SVD results is not a surprise. It will be difficult to obtain a unique UV−visible spectrum for this intermediate since it never builds up appreciably in solution. A further complication is that the kinetic system is highly coupled and it is difficult to determine unique sets of rate constants. The refined values for k_2, k_3, and k_8 obtained from the global fits have small statistical errors (1−3%), but they vary somewhat from run to run and we estimate uncertainties of up to ±100% based on replicates. This is not surprising for autocatalytic systems, especially in this case, owing to the small spectroscopic contribution from $Ru^{IV}ORu^{IV}$, the degree of cross-correlation, and the complexity of the kinetic model.

Disproportionation of $Ru^{V}ORu^{IV}$ at pH 0. As noted above, $Ru^{V}ORu^{IV}$ is thermodynamically stable with respect to disproportionation above pH 3. Since disproportionation to $Ru^{IV}ORu^{IV}$ and $Ru^{V}ORu^{V}$ gives $Ru^{V}ORu^{V}$, and is coupled to the irreversible oxidation of water, $Ru^{V}ORu^{IV}$ is ultimately thermodynamically unstable in this pH domain. However, solutions of $Ru^{V}ORu^{IV}$ prepared by bulk electrolysis of $Ru^{IV}ORu^{III}$ at $E_{app} > E_{1/2}$ ($Ru^{V}ORu^{IV}/Ru^{IV}ORu^{III}$) at 5 °C in acetate or phosphate buffer solutions (pH 3−6) are stable for several hours. Self-reduction is slow under these conditions.

The behavior of $Ru^{V}ORu^{IV}$ in acid solution was studied by adding acid to solutions of $Ru^{V}ORu^{IV}$ generated by the addition of stoichiometric HOCl to $Ru^{IV}ORu^{III}$ at pH 6.[12] Addition of sufficient acid to bring the pH to 0 after mixing at 25 °C causes an initial spectroscopic shift from 490 to 484 nm ($t_{1/2} < 10$ ms). This is followed by a complex sequence of coupled

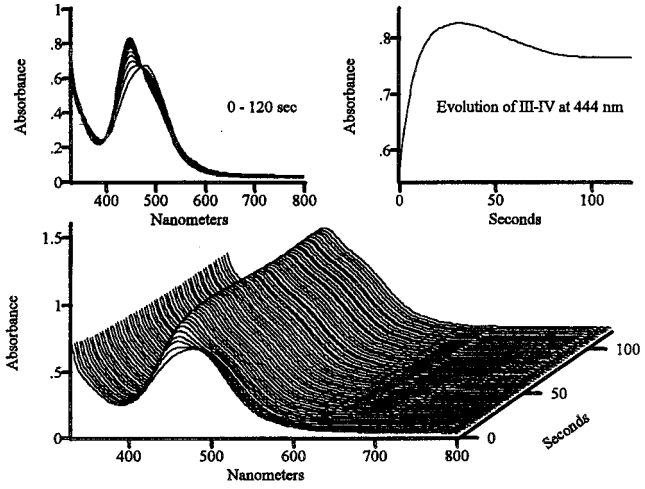

Figure 5.

reactions that involve second-order disproportionation and water oxidation.[24] Previous work by Raven and Meyer *incorrectly* attributed the initial slow following steps to *first-order* oxidation of water.[12] Our data, acquired over a wider time range, show that the process is clearly not first order. In addition, the concentration−time profile for the growth of $Ru^{IV}ORu^{III}$ matches that observed in experiments where $Ru^{V}ORu^{IV}$ is formed by Ce^{IV} addition, e.g., Figure 1, after consumption of Ce^{IV} is complete.

A more plausible explanation for the initial spectral change may be protonation. Lei and Hurst have obtained evidence for protonation of the μ-oxo bridge in $Ru^{V}ORu^{V}$ at pH 0 by use of resonance Raman spectroscopy.[15] The site of protonation is not known but the pK_a appears to lie between 0 and 1.

Oxidation of $Ru^{V}ORu^{IV}$ by Ce^{IV}. Multi-mixing experiments were pursued to investigate the kinetic behavior of $Ru^{V}ORu^{IV}$ with added Ce^{IV}. First, 2 equiv of Ce^{IV} was added to $Ru^{IV}ORu^{III}$ and allowed to react for 45 s before further addition of 2−10 equiv of Ce^{IV}. Following the second Ce^{IV} addition, a species appeared in solution whose spectrum matched that of $Ru^{IV}ORu^{III}$. This behavior is consistent with the full kinetic model, which includes the fact that entry into the catalytic cycle is rate limited by oxidation of $Ru^{IV}ORu^{III}$ to $Ru^{V}ORu^{IV}$. Once $Ru^{V}ORu^{IV}$ is reached, it is oxidized rapidly. This explains why the lower oxidation state is the predominant form even in the presence of a kinetic excess of Ce^{IV} (Figure 1).

In addition to the sequential, multi-mixing experiments, we studied the addition of 1−5 equiv of Ce^{IV} to solutions of $Ru^{V}ORu^{IV}$ that had been prepared electrochemically. In these experiments: (a) the acid medium contained the Ce^{IV}, (b) the mixing was performed manually with a T-mixer (Hamilton valve), and (c) the data were collected on an HP8452A diode array. The results of a typical experiment are shown in Figure 5.

The fact that $Ru^{IV}ORu^{III}$ appears much more rapidly than by the self-reduction of $Ru^{V}ORu^{IV}$, which is slow, proves that there is an oxidation state beyond $Ru^{V}ORu^{IV}$ that is the active catalyst for water oxidation at pH 0. The use of even a small excess of Ce^{IV} causes the system to enter the catalytic cycle in the same manner as described for the stopped-flow experiments. If there is excess Ce^{IV}, as in Figure 5, some catalytic activity is lost as evidenced by only partial oxidation of $Ru^{IV}ORu^{III}$ upon addition of a second aliquot of Ce^{IV}. Full reactivity was recovered after waiting at least $^1/_2$ h before addition of the second aliquot.

(24) Chronister, C. W.; Binstead, R. A. Unpublished results.

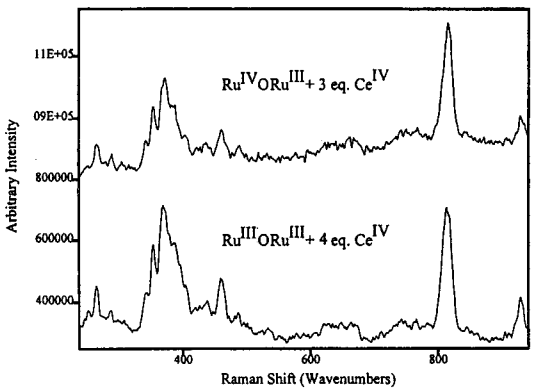

Figure 6.

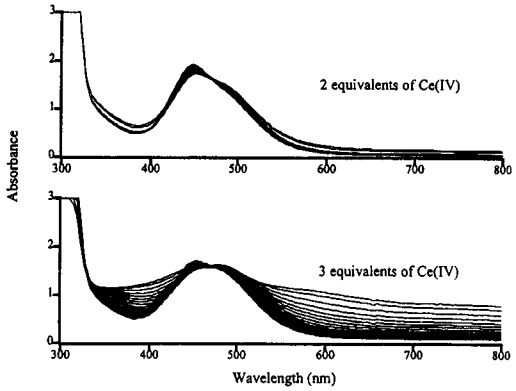

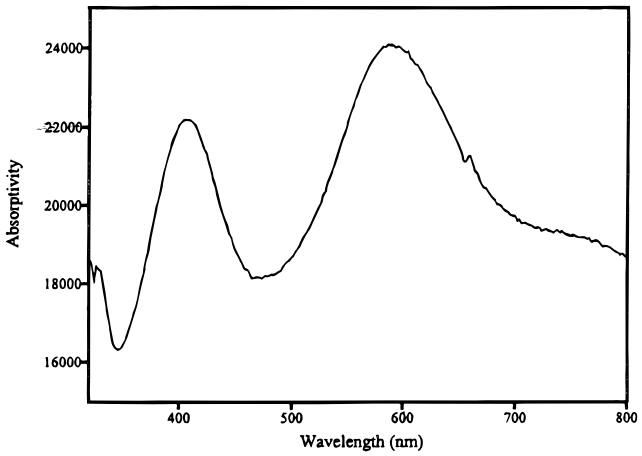

Figure 7.

As shown below, there is independent evidence for $Ru^{V}ORu^{V}$ as a viable oxidation state and intermediate in the oxidation of water. Even so, there is no evidence in the kinetics data for $Ru^{V}ORu^{V}$ as an intermediate when $Ru^{V}ORu^{IV}$ is oxidized by Ce^{IV}. Water oxidation by $Ru^{V}ORu^{V}$ must be rapid with $k_6 > 1$ s^{-1} if the reaction is assumed to be first order or $k_{6'} > 2 \times 10^4$ M^{-1} s^{-1} if second order (see below). Given these observations, it is plausible to assign the rate-limiting step for the net reaction in eq 2 to the oxidation of $Ru^{V}ORu^{IV}$ to $Ru^{V}ORu^{V}$ followed by the oxidation of water which is more rapid.

$$\left[\begin{array}{c} Ru^{V}-O-Ru^{IV} \\ \| \quad\quad | \\ O \quad\quad O \end{array}\right]^{3+} + 2\,Ce^{IV} + 2\,H_2O \longrightarrow \left[\begin{array}{c} Ru^{IV}-O-Ru^{III} \\ | \quad\quad | \\ HO \quad\quad OH_2 \end{array}\right]^{4+} + 2\,Ce^{III} + O_2 + H^+ \qquad (2)$$

With this interpretation and the data in Figure 5, $k_{obs} \sim 0.14$ s^{-1} for the appearance of $Ru^{IV}ORu^{III}$ at 444 nm. This corresponds to a second-order rate constant of $k' \sim 500$ M^{-1} s^{-1}, uncorrected for the stoichiometry of Ce^{IV} consumption. Ce^{IV} loss monitored at 360 nm was slower, giving an apparent rate constant of $k' \sim 100$ M^{-1} s^{-1}. This is consistent with slower Ce^{IV} oxidation of $Ru^{IV}ORu^{III}$ once the rapid reaction between $Ru^{V}ORu^{IV}$ and Ce^{IV} is complete. These results are consistent with the model developed to fit the stopped-flow kinetics data in Figure 3.

Characterization of $Ru^{V}ORu^{V}$. At 5 °C in 1 M $HClO_4$, addition of 3 equiv of Ce^{IV} to a 0.5 mM solution of $Ru^{IV}ORu^{III}$ results in the appearance of a black microparticulate suspension. No precipitate is formed at lower dimer concentrations or at higher temperatures with 3 equiv of added Ce^{IV}. Addition of 4 equiv of ascorbic acid to a cold solution containing the precipitate gave $Ru^{III}ORu^{III}$ and 3 equiv of $Ru^{IV}ORu^{III}$ consistent with retention of the μ-oxo bridge and formulation of the solid as a higher oxidation state. Resonance Raman studies on the black suspension prepared by stoichiometric Ce^{IV} oxidation of $Ru^{III}ORu^{III}$ or $Ru^{IV}ORu^{III}$ were conducted in frozen solutions at 77 K as described by Hurst and Lei.[14] Coupling of the IG-CCD detector to a Spex triplemate in the spectrograph mode allowed for the rapid measurement (minutes) of spectra eliminating problems caused by photoreduction of samples on the longer time scales required for data acquisition by conventional scanning systems.

After 1−2 h, the precipitated solid redissolved with formation of $Ru^{IV}ORu^{III}$ as shown by spectrophotometric measurements. By increasing the amount of time that passed between formation of the solid and freezing the solution prior to the Raman measurements, it was possible to obtain Raman spectra of the solid as a function of time. During the period that dissolution began, with $Ru^{IV}ORu^{III}$ appearing in the solution, the bands at 816 (ν_{sym}(Ru═O)) and ∼357 cm^{-1} (ν_{sym}(RuORu)) decreased in intensity and ν_{sym}($Ru^{IV}ORu^{III}$) at 398 cm^{-1} increased. During this period a broad band at 650 cm^{-1} also appeared in the spectrum of the suspension.

The suspension was also examined by UV−visible measurements, Figure 6b. The initial scan contained contributions from dissolved $Ru^{IV}ORu^{III}$ and $Ru^{V}ORu^{IV}$ in addition to the black suspension. By the end of the observation period (600 s) the precipitate had settled out. (**CAUTION**! The precipitate must be handled with extreme care because it is highly explosive. In one attempt to prepare a sample for IR measurements in a drybox, the solid ignited into a fire ball.) It also forms at room temperature with the dimer at high concentration ($\geq 5 \times 10^{-4}$ M) and Ce^{IV} in ≥100-fold excess.

SVD analysis of the spectral data in Figure 6b revealed the existence of five significant components. The data were reproduced very well by a multiexponential rate law (A → B → C → D → E). Although an oversimplification, a global fit to this model was useful as a way of extracting the spectrum of $Ru^{V}ORu^{V}$ in the solid suspension. The initial concentrations were set to account for the contributions of $Ru^{IV}ORu^{III}$ and $Ru^{V}ORu^{IV}$ at $t = 0$, resulting in the predicted spectrum shown in Figure 7. There is a large background offset in this spectrum due to light scattering, but the availability of even the qualitative data is useful as a guide to the general features in the spectrum. From this result it can be concluded that the apparent absorption bands near 400 and 600 nm, which do not appear in the spectra of $Ru^{III}ORu^{III}$, $Ru^{IV}ORu^{III}$, or $Ru^{V}ORu^{IV}$, arise from electronic transitions in $Ru^{V}ORu^{V}$.

Other Reactions. Multi-mixing experiments were also used to study the cross-reaction between $Ru^{V}ORu^{IV}$ and $Ru^{III}ORu^{III}$. In these experiments, 3 equiv of Ce^{IV} were added to $Ru^{III}ORu^{III}$ to generate $Ru^{V}ORu^{IV}$. This reaction was allowed to proceed for 45 s before further mixing with a solution containing Ru^{III}-ORu^{III}. The reaction was instantaneous (<1.25 ms) and produced only $Ru^{IV}ORu^{III}$ as an observable product, along with some unreacted $Ru^{III}ORu^{III}$. The net reaction is,

$$2Ru^{III}ORu^{III} + Ru^{V}ORu^{IV} \rightarrow 3Ru^{IV}ORu^{III} \qquad (3)$$

Based on this observation, and assuming second-order kinetics, $k \geq 10^6-10^7\ M^{-1}\ s^{-1}$. This and related cross-reactions involving $Ru^{V}ORu^{V}$ appear to play an important role in the kinetic behavior of the system under catalytic conditions (see below).

Loss of Catalytic Activity: Evidence for Anation. In 1 M $HClO_4$ or CF_3SO_3H, catalytic activity decreases with passage even through a single catalytic cycle. The effect is even more pronounced in 1 M HNO_3 or H_2SO_4. In these cases, passage through a single cycle can result in complete inhibition of catalysis, at least temporarily.

The effect also depends on reaction conditions. In 1 M $HClO_4$ or CF_3SO_3H with a large excess of Ce^{IV}, initial $Ru^{IV}ORu^{III}$ oxidation leads to rapid Ce^{IV} consumption but of only ~3−4 equiv. The initial rapid stage is followed by loss of Ce^{IV} by zero-order kinetics as shown in Figure 2. Decreasing the acid concentration to 0.1 M CF_3SO_3H or $HClO_4$ enhanced the rate of Ce^{IV} consumption past the initial, rapid stage. The kinetics are still roughly pseudo-zero order over much of the reaction but there is much greater curvature in the kinetic traces (Figure 1S in Supporting Information).

Addition of 10 equiv of Ce^{IV}, waiting 5 min for the Ce^{IV} to be depleted, and then adding an additional 2 equiv of Ce^{IV} resulted in oxidation of only ~50% of the available $Ru^{IV}ORu^{III}$ to $Ru^{V}ORu^{IV}$ as shown by UV−visible measurements. After waiting for periods as long as an hour, full reactivity toward Ce^{IV} was restored. Addition of stoichiometric Fe^{2+} reduces the inactive form of $Ru^{IV}ORu^{III}$ to $Ru^{III}ORu^{III}$ and restores full activity toward Ce^{IV}. The $Ru^{III}ORu^{III}$ form of the dimer is known to undergo ligand exchange more rapidly than $Ru^{IV}ORu^{III}$.[25]

These results can be explained by invoking anation induced by water oxidation. Anation is not a spontaneous event under these conditions and does not occur until sufficient Ce^{IV} is added to enter the catalytic cycle. Solutions containing either Ru^{III}-ORu^{III} or $Ru^{IV}ORu^{III}$ in 1 M $HClO_4$ or CF_3SO_3H are stable toward anation indefinitely. They retain the ability to be oxidized to $Ru^{V}ORu^{IV}$ and enter the water oxidation cycle without inhibition.

Discussion

The mechanism of water oxidation with $Ru^{III}ORu^{III}$ as the catalyst is kinetically complex. There are a series of sequential reactions which increase oxidative content in a stepwise manner beginning with $Ru^{IV}ORu^{III}$, ultimately reaching $Ru^{V}ORu^{V}$. Oxidation is accompanied by increased acidity and proton loss. Loss of protons is a key element since water oxidation requires loss of four electrons and four protons, ultimately with O−O bond formation, eq 1.

The kinetic studies point to rapid water oxidation by Ru^{V}-ORu^{V}, but at the high acid concentrations required to utilize Ce^{IV}, it is unsustainable. Passage through even a single catalytic cycle results in significant, if temporary, loss of catalytic activity because of anation induced by O_2 evolution, see below. The kinetics of Ce^{IV} consumption become zero order with the overall rate-limiting step aquation of the anated intermediate which then re-enters the catalytic cycle.

Chart 1[a]

Couple	Electron loss	Proton loss	$E_{1/2}$, V[a]
$[Ru^{IV}(HO)-O-Ru^{III}(OH_2)]^{4+} \rightarrow [Ru^{III}(H_2O)-O-Ru^{III}(OH_2)]^{4+}$	1	1	1.02
$\{Ru^{IV}-O-Ru^{IV}\}^{b} \rightarrow [Ru^{IV}(HO)-O-Ru^{III}(OH_2)]^{4+}$	2	3	> 1.45
$[Ru^{V}(O)-O-Ru^{IV}(O)]^{3+} \rightarrow \{Ru^{IV}-O-Ru^{IV}\}^{b}$			< 1.45
$[Ru^{V}(O)-O-Ru^{V}(O)]^{4+} \rightarrow [Ru^{V}(O)-O-Ru^{IV}(O)]^{3+}$	1	0	1.40

[a] At pH = 1 in 0.1 M CF_3SO_3H vs NHE. [b] Or $Ru^{V}ORu^{III}$, see text.

The net reaction in the catalytic cycle is oxidation of water to O_2 with Ce^{IV} as the terminal oxidant, eq 4. The dominant form of the catalyst under catalytic conditions is $Ru^{IV}ORu^{III}$ either because of rate-limiting oxidation or, as the reaction proceeds under catalytic conditions, rate-limiting aquation.

$$4Ce^{IV} + 2H_2O \xrightarrow{Ru^{IV}ORu^{III}} O_2 + 4Ce^{III} + 4H^{+} \qquad (4)$$

The mechanistic details of the individual steps will be discussed below. Each reaction, the associated loss of electrons and protons, and reduction potentials for the couples at pH 1 (measured as $E_{1/2}$ values by cyclic voltammetry) are summarized in Chart 1.

This listing emphasizes the stepwise loss of electrons and protons in reaching the active form. The loss of protons is required in the net reaction and has the advantage of avoiding charge buildup as electron content is decreased by oxidation. The listing also reveals the unusually high potential for one-electron oxidation of $Ru^{IV}ORu^{III}$ which is the origin of its thermodynamic instability toward disproportionation.[26] The catalyst itself acts as a molecular-level "transducer" in which a sequence of electron−proton-transfer steps leads to an activated form which has the ability to oxidize water by a multielectron step or steps involving atom transfer (see below).

Once $Ru^{V}ORu^{V}$ is reached, it is thermodynamically capable of water oxidation in a single four-electron step to give Ru^{III}-ORu^{III} and O_2, $\Delta G^{\circ} = -0.72$ eV for the reaction in eq f of Scheme 1. Although this suggests the adequacy of a single molecule to achieve water oxidation, the actual mechanism in solution appears to be bimolecular (see below).

Mechanism of Water Oxidation. In the oxidation of water starting with **1** there are three separate mechanistic stages: (1) oxidation of $Ru^{III}ORu^{III}$ to $Ru^{V}ORu^{V}$; (2) the evolution of O_2; and (3) suppression of catalysis by anation.

Oxidation of $Ru^{III}ORu^{III}$ to $Ru^{V}ORu^{V}$. Oxidation of Ru^{III}-ORu^{III} to $Ru^{V}ORu^{V}$ occurs by the series of steps in Scheme 1 and it is useful to discuss the separate reactions in turn.

(a) Oxidation of $Ru^{III}ORu^{III}$ to $Ru^{IV}ORu^{III}$. Given the known pK_{a1} values for $Ru^{III}ORu^{III}$ and $Ru^{IV}ORu^{III}$ in 1 M $HClO_4$, the dominant form of $Ru^{III}ORu^{III}$ is the diaqua complex, *cis,cis*-$[(bpy)_2(H_2O)Ru^{III}ORu^{III}(H_2O)(bpy)_2]^{4+}$. $Ru^{IV}ORu^{III}$ exists as an equilibrium mixture of *cis,cis*-$[(bpy)_2(H_2O)Ru^{IV}ORu^{III}$-$(H_2O)(bpy)_2]^{5+}$ and *cis,cis*-$[(bpy)_2(HO)Ru^{IV}ORu^{III}(H_2O)(bpy)_2]^{4+}$.

(25) Doppelt, P.; Meyer, T. J. *Inorg. Chem.* **1987**, *26*, 2027.

(26) Lebeau, E. L.; Adeyemi, S. A.; Meyer, T. J. *Inorg. Chem.* **1998**, *37*, 6476.

The kinetics of oxidation of the first stage are first order in $Ru^{III}ORu^{III}$ and Ce^{IV} with the net reaction,

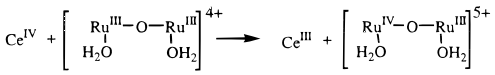

(5)

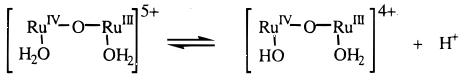

The rate constant for this reaction decreases by ~1/3 when the acid concentration is decreased by 10, is slightly more rapid in CF_3SO_3H than in $HClO_4$, and there is a slight but reproducible inverse D_2O/H_2O kinetic isotope effect of 0.87 in 1.0 M CF_3SO_3H and 0.82 in 0.1 M CF_3SO_3H, Table 1. It was not possible to extend the pH range in the kinetics study because of hydrolysis of Ce^{IV}. Attempts to unravel pH and ionic strength effects separately were unsuccessful because of precipitation.

It may be possible to account for the inverse isotope effect by invoking an acid−base preequilibrium at $Ru^{III}ORu^{III}$ or the hydrolysis of Ce^{IV} to give $CeOH^{3+}$, but there is no evidence for rate acceleration as the pH is increased from 0 to 1. The mechanism of this reaction is presumably outer-sphere electron transfer.

(b) Oxidation of $Ru^{IV}ORu^{III}$ to $Ru^{V}ORu^{IV}$. This is the slow step in the oxidation mechanism. Since Ce^{IV} is a one-electron oxidant, the oxidation of $Ru^{IV}ORu^{III}$ to $Ru^{V}ORu^{IV}$ must occur stepwise through a one-electron intermediate, $Ru^{IV}ORu^{IV}$. There is only inferential evidence for $Ru^{IV}ORu^{IV}$ in the kinetics. This is predicted by the rate constants in Scheme 1 which show that $Ru^{IV}ORu^{IV}$ never builds up to a significant extent in solution.

The intermediate $Ru^{IV}ORu^{IV}$ is unstable toward disproportionation showing that for the couples in eqs 6a and 6b, $E_{1/2}(1) > E_{1/2}(2)$.

$$Ru^{IV}ORu^{IV} + e \rightarrow Ru^{IV}ORu^{III} \qquad E_{1/2}(1) \qquad (6a)$$

$$Ru^{V}ORu^{IV} + e \rightarrow Ru^{IV}ORu^{IV} \qquad E_{1/2}(2) \qquad (6b)$$

Thermodynamically, it is easier to oxidize $Ru^{IV}ORu^{IV}$ to $Ru^{V}ORu^{IV}$ than it is to oxidize $Ru^{IV}ORu^{III}$ to $Ru^{IV}ORu^{IV}$. This explains why $k_2 < k_4$ in Scheme 1 and why oxidation of $Ru^{IV}ORu^{III}$ is rate-limiting in catalysis.

As slow $Ru^{IV}ORu^{III}$ oxidation by Ce^{IV} proceeds, $Ru^{V}ORu^{IV}$ begins to build up in solution and a new pathway intervenes for reaching $Ru^{IV}ORu^{IV}$. It involves comproportionation between $Ru^{V}ORu^{IV}$ and $Ru^{IV}ORu^{III}$, to give $Ru^{IV}ORu^{IV}$, eq c in Scheme 1. Even though this reaction is thermodynamically disfavored, it begins to dominate after a short induction period which explains the autocatalytic behavior in the absorbance−time traces in Figure 4.

The origin of the thermodynamic instability of $Ru^{IV}ORu^{IV}$ is unclear. In the related tetraaqua dimer $[(tpy)(H_2O)_2Ru^{III}ORu^{III}(H_2O)_2(tpy)]^{4+}$, the sequential oxidation of $Ru^{III}ORu^{III}$ to $Ru^{V}ORu^{V}$ occurs in the expected order with $E_{1/2}(1) = 1.04$ V (vs NHE in 1 M $HClO_4$) and $E_{1/2}(2) = 1.54$ V.[26]

Even the proper oxidation state description for this intermediate is unclear. It could be $Ru^{V}ORu^{III}$ given the known example of *cis*,*cis*-$[(bpy)_2(O)Ru^{V}ORu^{III}(py)(bpy)_2]^{4+}$,[25] or $Ru^{IV}ORu^{IV}$, probably as the dihydroxo form, *cis*,*cis*-$[(bpy)_2(HO)Ru^{IV}ORu^{IV}(OH)(bpy)_2]^{4+}$. In either case, it seems reasonable to suggest that in the oxidation of $Ru^{IV}ORu^{III}$ to $Ru^{V}ORu^{IV}$, the first step involves loss of one electron and one proton,

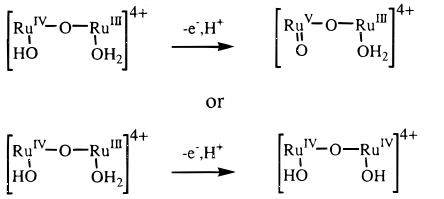

and the second, loss of one electron and two protons, e.g.,

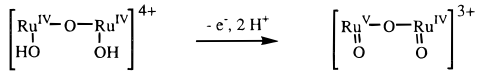

(7)

(c) Oxidation of $Ru^{V}ORu^{IV}$ to $Ru^{V}ORu^{V}$. There is independent spectroscopic evidence for $Ru^{V}ORu^{V}$ in the insoluble suspension that forms upon oxidation with Ce^{IV} at 0 °C in 1 M $HClO_4$, even though it does not appear as a detectable intermediate in solution.

The spectroscopic data on the suspension are revealing as to molecular structure. The intense absorption bands at ~410 and ~590 nm, with a shoulder at 760 nm, are consistent with retention of the μ-oxo bridge and $\pi \rightarrow \pi^*$ transitions localized on the RuORu bridge.[12] Direct evidence for retention of the μ-oxo bridge is provided by the resonance Raman data and the appearance of ν_{sym}(Ru−O−Ru) at 357 cm^{-1}. In addition, a band appears at 816 cm^{-1} for a terminal ν(Ru═O) stretch. These results are in good agreement with those obtained by Lei and Hurst in solutions that were frozen to 90 K after addition of excess oxidant.[15] Analogous ν(Ru═O) stretching bands appear at 792 and 834 cm^{-1} in *cis*-$[Ru^{IV}(bpy)_2(py)(O)]^{2+}$ and *trans*-$[Ru^{IV}(tpy)(O)_2(H_2O)]^{2+}$, respectively.[27,28] The terminal oxo formulation is also consistent with the pH-dependent electrochemical measurements mentioned earlier.[11]

Mechanism of O_2 Evolution. Water oxidation is triggered by oxidation of $Ru^{V}ORu^{IV}$ by Ce^{IV} which occurs with $k \sim 400$ M^{-1} s^{-1}. $Ru^{V}ORu^{V}$ is an intermediate, and can be trapped as its ClO_4^- salt at 5 °C, but there is no direct kinetic information about its rate of water oxidation.

In the reaction between $Ru^{V}ORu^{IV}$ and Ce^{IV} to give $Ru^{IV}ORu^{III}$ and O_2, eq 2, there is no fundamental mechanistic information in the appearance of $Ru^{IV}ORu^{III}$ as the initial product. Even if the reaction occurred by an intramolecular, four-electron step,

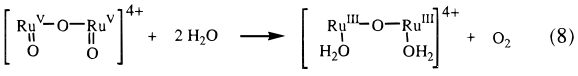

(8)

$Ru^{IV}ORu^{III}$ would be the initial product because of rapid cross-electron transfer between $Ru^{III}ORu^{III}$ and $Ru^{V}ORu^{IV}$ (reaction g in Scheme 1) or with $Ru^{V}ORu^{V}$.

In Scheme 1 it is assumed for modeling purposes that O_2 evolution is first order in $Ru^{V}ORu^{V}$. This may actually be a bimolecular reaction. There is evidence that water oxidation by the $Ru^{V}ORu^{V}$ form of $[(tpy)(H_2O)_2Ru^{III}ORu^{III}(H_2O)_2(tpy)]^{4+}$ is bimolecular.[26]

The results of an earlier ^{18}O-labeling experiment are also qualitatively consistent with a bimolecular mechanism.[13] In this experiment, oxidation of ^{18}O-labeled $Ru^{IV}ORu^{III}$ in $H_2{}^{16}O$ in 0.1 M CF_3SO_3H by Ce^{IV} gave the product distribution illustrated in eq 9. By inference, the remaining 1.1 out of 2.0 ^{18}O atoms

(27) Moyer, B. A.; Meyer, T. J. *J. Am. Chem. Soc.* **1978**, *100*, 3601.
(28) Adeyemi, S. A.; Dovletoglou, A.; Guadalupe, A. R.; Meyer, T. J. *Inorg. Chem.* **1992**, *31*, 1375.

remained in the coordination sphere of $Ru^{IV}ORu^{III}$. (A different

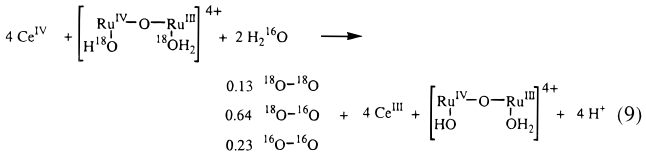

result was obtained in later work by Hurst and Lei with Co^{3+} as the oxidant in 1 M CF_3SO_3H. They obtained only trace $^{18}O-^{18}O$, ~0.4 $^{18}O-^{16}O$, and ~0.6 $^{16}O-^{16}O$. There is no reason to believe that the earlier work was incorrect.[13])

Assuming a single pathway for water oxidation, the ^{18}O-labeling result would appear to rule out intramolecular oxidation with O_2 coming from a single $Ru^{V}ORu^{V}$. If that were the case, the only labeled O_2 product would be $^{18}O-^{18}O$ by the mechanism,

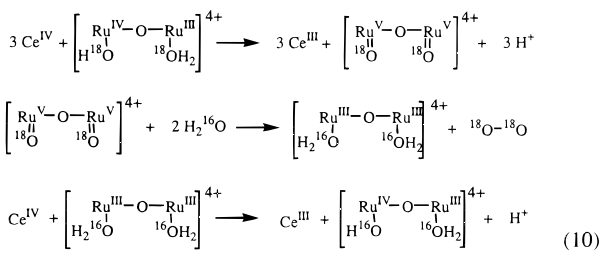

The appearance of $^{16}O-^{16}O$ could be explained by a scrambling of the ^{18}O label in a cross-reaction between $Ru^{V}ORu^{V}$ and $Ru^{IV}ORu^{III}$,

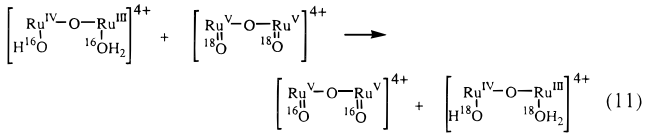

or between $Ru^{V}ORu^{IV}$ and $Ru^{IV}ORu^{III}$, eq c in Scheme 1. It is not possible to account for $^{18}O-^{16}O$ as a product by this mechanism.

The appearance of $^{18}O-^{16}O$ by the intramolecular mechanism could still be explained, as suggested by a reviewer, if there is partial oxo-exchange with $H_2{}^{16}O$ on the time scale for water oxidation.

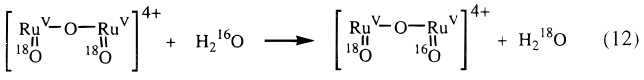

The appearance of $^{18}O-^{16}O$ could also be explained by a mechanism in which a water molecule attacks an oxo group,

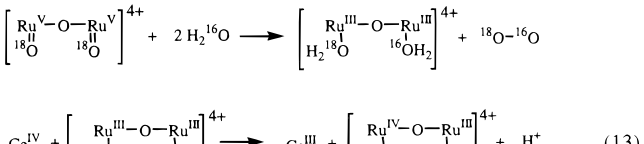

but this mechanism cannot explain $^{18}O-^{18}O$ as a product.

As explained by Geselowitz et al.,[13] the appearance of all three labeled forms can also be explained, at least qualitatively, by invoking a bimolecular mechanism and the first step in eq 14.

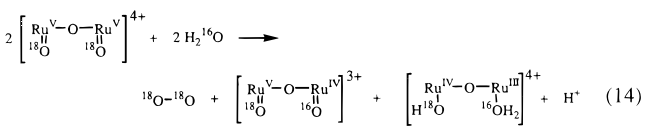

The next cycle, following reoxidation to $Ru^{V}ORu^{V}$, would occur by,

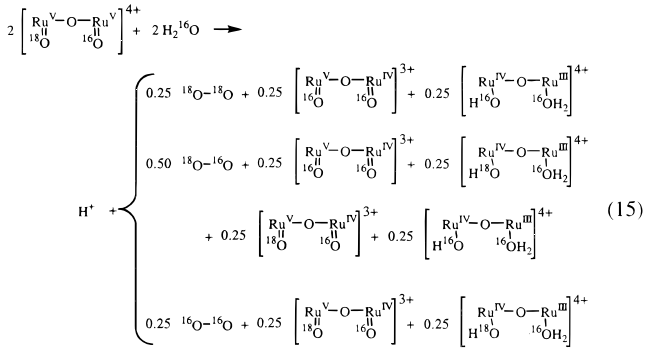

This mechanism cannot explain the $^{18}O-^{16}O$-rich product distribution. To explain this result it is necessary to invoke ^{16}O incorporation by cross-reactions between the ^{16}O forms of $Ru^{IV}ORu^{III}$ and the ^{18}O forms of $Ru^{V}ORu^{V}$ and/or $Ru^{V}ORu^{IV}$.

The labeling result could also be explained if there is more than one contributing pathway. If the reaction does involve the bimolecular pathway, under the conditions in Figure 4 with $[Ru^{V}ORu^{V}] = 5 \times 10^{-5}$ M and $t_{1/2} \leq 1$ s, $k_6' \geq 2 \times 10^4$ M^{-1} s^{-1}. If the reaction is intramolecular, $k_6 \geq 1$ s^{-1}. In either case, this analysis shows that the intrinsic reactivity of $Ru^{V}ORu^{V}$ toward water oxidation is high.

It is interesting to speculate about the microscopic details by which O_2 is evolved. In Scheme 2 a two-stage mechanism is proposed assuming a bimolecular reaction in which a symmetrical μ-peroxo intermediate forms initially. There is no evidence for such an intermediate in solution, but in the solid-state decomposition of $Ru^{V}ORu^{V}$ to give $Ru^{IV}ORu^{III}$ and O_2 there is evidence for a new feature in the resonance Raman spectrum at 650 cm^{-1}.

Similarly, an intramolecular mechanism could involve the formation of a μ-oxo-μ-peroxo intermediate. There is consider-

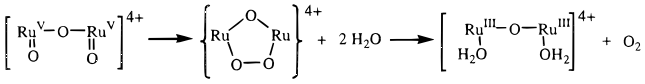

able literature precedence for such a structure.[32−34] As in the bimolecular mechanism, subsequent loss of O_2 would occur promoted by water attack, to give $[(H_2O)Ru^{III}ORu^{III}(OH_2)]^{4+}$.

The evidence for an intermediate in the solid state may be an important observation, especially given the resonance Raman results of Que et al. on a series of $Fe^{III}Fe^{IV}$ complexes, $[Fe_2(\mu\text{-}O)_2L_2](ClO_4)_3$, which contain the $Fe_2(\mu\text{-}O)_2$ core and a

(29) Wilkinson, E. C.; Dong, Y.; Zang, Y.; Fujii, H.; Fraczkiewicz, R.; Fraczkiewicz, G.; Czernuszewicz, R. S.; Que, L., Jr. *J. Am. Chem. Soc.* **1998**, *120*, 955.

(30) Pidcock, E.; DeBeer, S.; Obias, H. V.; Hedman, B.; Hodgson, K. O.; Karlin, K. D.; Solomon, E. I. *J. Am. Chem. Soc.* **1999**, *121*, 1870.

(31) Tolman, W. B. *Acc. Chem. Res.* **1997**, *30*, 227.

(32) Bhula, R.; Gainsford, G. J.; Weatherburn, D. C. *J. Am. Chem. Soc.* **1988**, *110*, 7550.

(33) Micklitz, W.; Bott, S. G.; Bentsen, J. G.; Lippard, S. J. *J. Am. Chem. Soc.* **1989**, *111*, 372.

(34) Bossek, U.; Weyhermüller, T.; Wieghardt, K. *Inorg. Biochem.* **1991**, *43*, 371.

Scheme 2

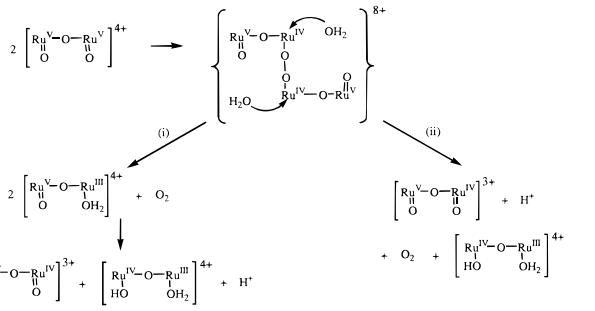

Scheme 3

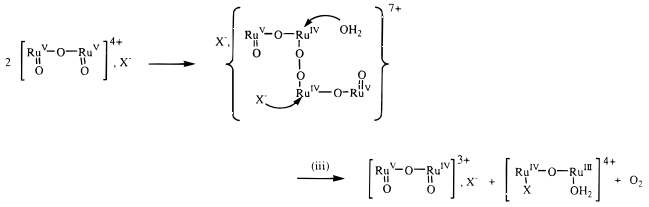

tetradentate ligand L. A band appears in these spectra at 667 cm^{-1} which was assigned to ν_2, the t_{2g} mode of the C_{2h} $Fe_2(\mu\text{-}O)_2$ core.[29] With this observation as a guide, the solid-state intermediate may have a related di-μ-oxo structure (see below) rather than the linear structure implied in Scheme 2. This structural motif is well recognized in dimeric $Cu-O_2$ complexes.[30,31]

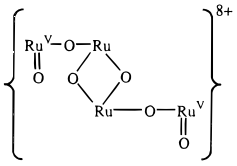

The second step in Scheme 2 is intramolecular electron transfer which can occur: (1) symmetrically to give $Ru^{IV}ORu^{IV}$ (shown as $[(O)Ru^{V}ORu^{III}(OH_2)]^{4+}$), followed by disproportionation (path i), or (2) asymmetrically to give $Ru^{V}ORu^{IV}$ and $Ru^{IV}ORu^{III}$ (path ii). In the latter case, the last two electrons from the μ-peroxo bridge are transferred to only one of the bridged partners. It has the advantage of forming thermodynamically more stable products. The suggestion of electron transfer promoted by water attack in Scheme 2 provides a means for avoiding the lower coordinate, higher energy intermediates that would result from unpromoted loss of O_2.

Anation: Suppression of Catalysis. The loss of catalytic activity can be attributed to anation induced by O_2 evolution. Anation has been observed in related systems.[18,26] It is probably a consequence of ion-pairing with the $[(O)Ru^{V}ORu^{V}(O)]^{4+}$ cation during the O_2 evolution step. Anated products would result by competitive anion capture of a coordination site as shown in Scheme 3. The resulting anated form of $Ru^{IV}ORu^{III}$, $[(X)Ru^{IV}ORu^{III}(OH_2)]^{4+}$ ($X = ClO_4$, CF_3SO_3), would no longer have the two coordinated water molecules required to reach $Ru^{V}ORu^{IV}$. This formulation also explains why only very slight UV−visible spectral shifts are observed when catalysis is suppressed, Figure 1. The spectra of the intermediates should be very close to that of $[(HO)Ru^{IV}ORu^{III}(OH_2)]^{4+}$.

After a few passages through the water oxidation cycle, conversion to the anated complex appears to be complete. Under these conditions, the rate-determining step for water oxidation is aquation,

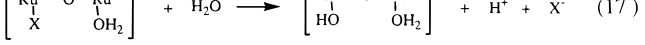

(17)

followed by the sequence of steps starting at eq b in Scheme 1. In this interpretation the rate constants, $k = 0.01\ s^{-1}$ in 1 M CF_3SO_3H and $0.025\ s^{-1}$ in 1 M $HClO_4$, derived by analysis of the pseudo-zero slopes from data such as those in Figure 3, are a measure of the relative rate constants for aquation for the two anions.

This interpretation explains the zero-order dependence of the Ce^{IV} loss kinetics in Figure 3 since Ce^{IV} loss follows rate-determining aquation. The first-order dimer dependence on Ce^{IV} consumption reported by Hurst and Lei is also understandable since the available $Ru^{IV}ORu^{III}$ at any time depends linearly on the initial concentration of the anated intermediate. Anation/aquation can also explain the loss of clean pseudo-zero-order kinetic behavior as the total anion concentration is decreased from 1.0 to 0.1 M. In more dilute solutions, ion-pairing is less complete and less of the anated form of the dimer is produced with each passage through a catalytic cycle.

Conclusions and Final Comments

The Ru μ-oxo dimer shares some common features with the Mn-containing oxygen-evolving complex (OEC) of photosynthesis. In both, sequential loss of four electrons leads to a high oxidation state form which is activated toward water oxidation. Both appear to share common structural motifs including μ-oxo bridging and terminal aqua ligands.

Available EXAFS data on the OEC point to a structure containing two linked μ-oxo dimeric subunits which provide the mechanistic basis for water oxidation.[2] For the Ru complex, a dimer of dimers may also be involved, but it is formed by diffusion in a bimolecular reaction where the critical step may be O···O coupling and formation of a O−O peroxo intermediate. Subsequent intramolecular electron transfer from the bridging ligand to Ru, perhaps promoted by H_2O attack, gives O_2. If the mechanism is bimolecular, there may be a significant mechanistic advantage in distributing the activational requirements for O−O bond formation over two dimers rather than one.

There may also be lessons about the OEC in the redox properties of the Ru dimer. One is the importance of proton loss coupled to electron loss, Chart 1. This has the effect of avoiding charge buildup and helps meet the ultimate requirement of loss of both protons and electrons for water oxidation.

The rate constant data point to a reactivity toward water oxidation for the Ru dimer that is impressive. This suggests that it may be possible to create catalysts in which the kinetic barrier to O_2 evolution is surprisingly low. There are other challenges to contend with in catalyst design. A coordination environment must be chosen that can survive the strongly oxidizing conditions required for water oxidation. There also appears to be a requirement for at least one aqua ligand to provide access to an oxo group by oxidation and proton loss. This is true at least for pathways that do not involve formation of intermediate hydroxyl radicals.

Multiple pathways for H_2O oxidation may exist and play an important role. The bimolecular mechanism, the intramolecular mechanism in eq 8, and H_2O attack on an oxo group in eq 12 are all reasonable pathways and may contribute or even dominate in other molecules.

There are clear lessons learned here about the design of catalysts for H_2O oxidation. One is the disadvantage of a high

positive charge with the associated ion-pairing that occurs in the strongly acidic solutions required to use Ce^{IV} as an oxidant. This leads to catalyst inhibition due to anation induced by O_2 evolution. Another is the advantage of preparing dimer-of-dimer structures which have the ability to promote inter-unit O···O coupling.[35] The design of modified Ru dimer structures incorporating appropriate design features is currently under investigation.

(35) Petach, H. H.; Elliott, C. M. *J. Electrochem. Soc.* **1992**, *139*, 2217.

Acknowledgment. We thank the National Institutes of Health for financial support of this work under Grant No. 5-R01-GM32296-11. We also thank Prof. Kenneth Karlin of Johns Hopkins University a helpful discussion.

Supporting Information Available: Supplementary Figures 1S−3S (PDF). This material is available free of charge via the Internet at http://pubs.acs.org.

JA993235N